Fluid evolution of the Paleoproterozoic Hujiayu copper deposit in the Zhongtiaoshan region: Evidence from fluid inclusions and carbon–oxygen isotopes

Yuhang Jiang [a,b], Hecai Niu [a,*], Zhiwei Bao [a], Ningbo Li [a,b], Qiang Shan [a], Wubin Yang [a], Shuang Yan [a,b]

[a] Key Laboratory of Mineralogy and Metallogeny, Guangzhou Institute of Geochemistry, Chinese Academy of Sciences, Guangzhou 510640, China
[b] University of Chinese Academy of Sciences, Beijing 100049, China

ABSTRACT

The Zhongtiaoshan region, located in the southern margin of the North China Craton, is the host to a number of metamorphosed sediment-hosted stratiform copper deposits. These deposits are hosted by dolomitic marble and silicic albitite of the mid-Paleoproterozoic Zhongtiao Group and contain economically significant copper and cobalt. The formation of these deposits is considered to be closely associated with the evolution of the Paleoproterozoic "Zhongtiao" rift. The Hujiayu deposit, the second largest Cu deposit of this type, is mainly hosted in silicic albitite and dolomitic marble in the upper part of the Bizigou Formation but locally extends into carbonaceous shales at the bottom of the Yujiashan Formation. Mineralization of the Hujiayu Cu deposit can be divided into an early stage (diagenetic stage) with disseminated to veinlet sulfides and a late stage (metamorphism stage) with coarse-vein sulfides. Mineral assemblages are similar for the two stages, with major minerals as chalcopyrite, pyrite, and pyrrhotite and main gangue minerals as dolomite and quartz. Sulfide veinlets formed in the early stage are thin and discrete, and have irregular boundaries with the host rocks; whereas the ore-bearing veins of the late stage are controlled by fractures.

Five types of fluid inclusions are recognized in the Hujiayu Cu deposit and they are: (1) pure vapor and vapor-rich inclusion (V-type), (2) pure CO_2 inclusion (PC-type), (3) CO_2–H_2O inclusion (C-type), (4) liquid-rich inclusion (L-type), and (5) daughter mineral-bearing inclusion (S-type). Microthermometric analysis shows that the ore-forming fluids of the early mineralization stage are characterized by high salinity (22–40 wt.% NaCl equiv.) and moderate temperature (120–280 °C). The ore-forming fluids of the late mineralization stage are characterized by CO_2 enrichment, high salinity, high temperature and underwent significant unmixing at a temperature interval of 240–480 °C. Compositions of the ore-forming fluids in the early and late stages are interpreted to be mainly basinal brine and metamorphic hydrothermal solution, respectively. Carbon and oxygen isotope compositions suggest possible carbon isotope exchange between the ore-forming fluids and organic-rich carbonaceous shales during the early stage. In the late mineralization stage, both degassing of CO_2 and isotopic exchange with organic carbon may have contributed to the formation of the more negative $\delta^{13}C_{V\text{-PDB}}$ values of mineralized carbonates.

The early stage mineralization of the Hujiayu Cu deposit may have occurred via interaction of oxidized Cu-bearing brines from the red-bed in the lower segment of the Bizigou Formation with the overlying reductive carbonaceous shales. Late stage mineralization at Hujiayu was mainly triggered by CO_2 escaping from metamorphic hydrothermal solutions.

1. Introduction

Sediment-hosted stratiform copper deposits are an important type of Cu resource globally, constituting approximately 23% of the world's discovered copper (Singer, 1995; Hitzman et al., 2010). They are formed in evolving basin-scale fluid-flow systems and are comprised of disseminated and veined copper and copper-iron

sulfide mineralization in dolomitic or silica clastic sedimentary rocks (Brown, 1997; Hitzman et al., 2005). It is widely accepted that the migration of oxidized ore-bearing fluids into a reducing environment leads to the precipitation of ore minerals (Rose, 1976; Brown, 1992; Hitzman et al., 2010). However, details of the ore-forming fluid system are still unclear (Hitzman et al., 2005, 2010), mainly due to the absence of syn-ore gangue minerals that contain fluid inclusions representative of the ore-forming fluids (Hitzman et al., 2010).

The Hujiayu copper deposit is located in the Zhongtiaoshan region on the southern margin of the North China Craton. The Hujiayu copper deposit is geologically similar to the nearby Bizigou, Laobaotan, and Tongmugou deposits (Fig. 1) and is classified as a "Hu-Bi type" copper deposit in literature (CGGCDZM, 1978; Sun and Hu, 1993). The "Hu-Bi type" copper deposits are similar to sediment-hosted Cu deposits in many respects. They are stratiform orebodies composed of disseminated and veined Cu and Cu–Fe sulfides. The orebodies are hosted within dolomitic marble and carbonaceous shales of the mid-Paleoproterozoic Zhongtiao Group (Sun and Hu, 1993). Red beds composed of weakly metamorphosed hematitic siltstone and dolomitic marble underlie the stratiform orebodies (Wei et al., 1984). Many studies have been conducted on the statistical interpretation of microthermometry and H–O–C isotope compositions regarding the ore-forming fluids of the Hu-Bi type deposits (Sun and Ge, 1990; Zhen et al., 1995; Pang, 2010; Huang et al., 2013). In this paper, we focus on the syn-ore quartz and dolomite of the early stage and ore-bearing quartz-dolomite veins of the late stage. Using field and petrographic observations, microthermometric analyses, laser Raman spectroscopy analyses and carbon–oxygen isotopic study, the composition, origin, and evolution of the ore-forming fluids at the Hujiayu copper deposit as well as their implications on ore formation are discussed.

2. Regional geology

The Zhongtiaoshan region is located in the south segment of the Trans-North China Orogen (Zhao et al., 2001; Liu et al., 2012). A Paleoproterozoic "Zhongtiao" rift has been form in this region (Sun and Hu, 1993; Sun et al., 1995; Zhen, 1997; Fig. 1). More than 30 copper deposits in the Zhongtiaoshan area are believed to have been formed during the evolution of "Zhongtiao" rift. This yields a total metal endowment of approximately 400 Mt of metal Cu (Xu, 2010).

The Precambrian strata exposed in the Zhongtiaoshan area include, from the oldest to the youngest, the Sushui Complex, Jiangxian Group, Zhongtiao Group, Danshanshi Group, and Xiyanghe Group (Hu and Sun, 1987; Sun and Ge, 1990; Bai, 1997; Fig. 1B). The Sushui Complex, the oldest rock unit identified in the Zhongtiaoshan area, consists mainly of the Neoarchean (2.8–2.5 Ga) TTG gneiss (Sun and Hu, 1993; Tian et al., 2006; Zhao et al., 2012a; Liu et al., 2012; Zhu et al., 2013; Wan et al., 2014). Rifting in the Zhongtiaoshan area began at approximately 2.2–2.1 Ga. The North China Craton in this period was in an extensional regime (Zhai et al., 2010; Zhai and Santosh, 2011, 2013), which lead to abundant magmatism in the Trans-North China Orogen (Du et al., 2010, 2012). The accumulation of potassic bimodal volcanic rocks and shallow facies clastic sedimentation in this period formed the Jiangxian Group, which hosts Luojiahe Cu deposit (Jiang et al., 2013b). As the rifting entered intermediate stage at 2.1 Ga, the sedimentation was primarily terrigenous clastic, volcanic, and marine carbonate, forming the Zhongtiao Group (Sun and Ge, 1990; Sun and Hu, 1993). The first phase of the "Zhongtiao" movement, occurring at ∼1.9 Ga (Sun and Hu, 1993; Zhang, 2012), may have led to the closure of the "Zhongtiao" rift. At ∼1.85 Ga, the collision between the Eastern and

Western Blocks formed the Trans-North China Orogen (Liu et al., 2012).

The "Zhongtiao" rift is a triple junction rift system with intense fracturing (Fig. 1). The NE-trending branch near the continent failed during the evolution of the rift. The SE-trending and SW-trending basement fractures controlled the emplacement of the stratiform Cu deposits such as the Tongkuangyu, Luojiahe, and the Hu-Bi type Cu deposits (Sun et al., 1995; Fig. 1).
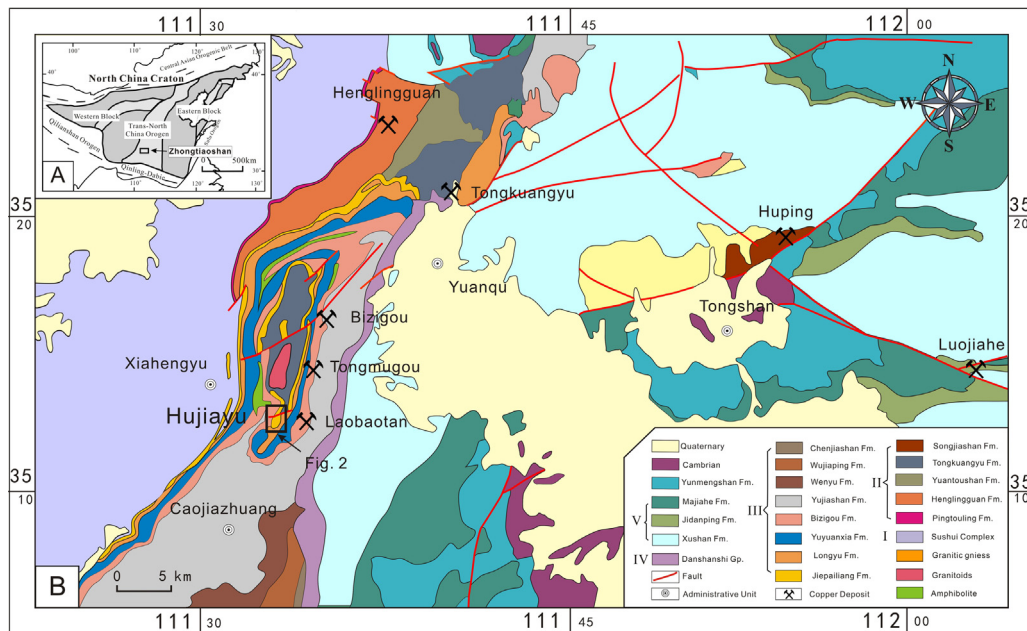
3. Ore geology

Many sediment-hosted stratiform Cu deposits in the Zhongtiaoshan region are hosted in the Zhongtiao Group. The majority of the deposits occur in silicic albitite and dolomitic marble between the lower parts of the Yujiashan Formation and the top of the Bizigou Formation (CGGCDZM, 1978; Sun et al., 1995; Fig. 2). The Bizigou, Hujiayu, Tongmugou, and Laobaotan Cu deposits, four typical "Hu-Bi type" deposits, are located in an approximately 20 km long belt in the southwest branch of the "Zhongtiao" rift (Fig. 1B). The Bizigou Cu deposit, containing 393, 591 *t* copper (average Cu grade: 1.492%) and 1, 844 *t* Co (average Co grade: 0.024%), is the largest "Hu-Bi type" deposit (Huang et al., 2001). The Hujiayu Cu deposit is located 12 km south of Bizigou (Fig. 2), with reserves of approximately 320,000 *t* Cu (average Cu grade: 1.07%), 1700 *t* Co (average Co grade: 0.027%), 1.119 *t* Au (average grade 0.19 *g*/*t* Au), and 10 *t* Ag (average grade 1.25 *g*/*t* Ag) (Huang et al., 2001). The Hujiayu mine comprises of 167 orebodies. Number 3 is the largest and is 650 m long and 24 m thick (Sun et al., 1995).

The strata exposed in the Hujiayu mining area include the Yuyuanxia, Bizigou, and Yujiashan Formations (from the oldest to the youngest) (Fig. 2A). The Yuyuanxia Formation is composed predominantly of stromatolite-bearing dolomitic marble. The orebodies are mainly hosted in the Bizigou Formation. The rocks of the Bizigou Formation are generally classified into six types (the deepest to the shallowest): amphibolite, scapolite–biotite schist, red sandstone and dolomitic marble, gray dolomitic marble, silicic albitite, and carbonaceous shales (Fig. 3C). The orebodies are mainly hosted in the silicic albitite and gray dolomitic marble within the upper segment of the Bizigou Formation, but they locally extend into the unraninite and pyrite bearing carbonaceous shales (Figs. 3A and 4A) at the bottom of the Yujiashan Formation. The silicic albitite is spatially associated with dolomitic marble and carbonaceous shales, and is characterized by very fine stratification consisting of albite and quartz. The presence of red beds is ubiquitous in the Zhongtiao Group although its importance is often ignored (Wei et al., 1984; Cen, 1993). The red beds (red dolomitic marble and sandstone) occur discontinuously in the lower segment of the Bizigou Formation with a total thickness of up to one hundred meters (Wei et al., 1984; Fig. 3D). However, the thickness of the individual red beds ranges from 6 to 20 m. The occurrence of red beds is similar to other strata of the Bizigou Formation. Strongly limonitic dolomitic marble can be observed in some parts of the Bizigou Formation.

Fold and fault structures are well-developed in the Hujiayu mine area. The Nanhegou-Xigou congruent inverted syncline is the main structural control of the orebodies (Fig. 2A). Common types of hydrothermal alteration products observed at the Hujiayu Cu deposit include albite, carbonate, biotite, and silica. However, the alteration associated with mineralization can be difficult to identify because post-mineralization regional metamorphism also significantly altered the rocks of Bizigou Formation (CGGCDZM, 1978; Sun and Ge, 1990).

The mineralization observed in the Hujiayu Cu deposit can be divided into early stage (diagenetic stage) and late stage (metamorphic stage):

Fig. 1. Regional geological map of the Zhongtiaoshan area. (A). Tectonic framework of the North China Craton and the location of Zhongtiaoshan. (B). Regional geology of the Zhongtiaoshan area. I – Sushui Complex; II – Jiangxian Group; III – Zhongtiao Group; IV – Danshanshi Group; V – Xiyanghe Group.
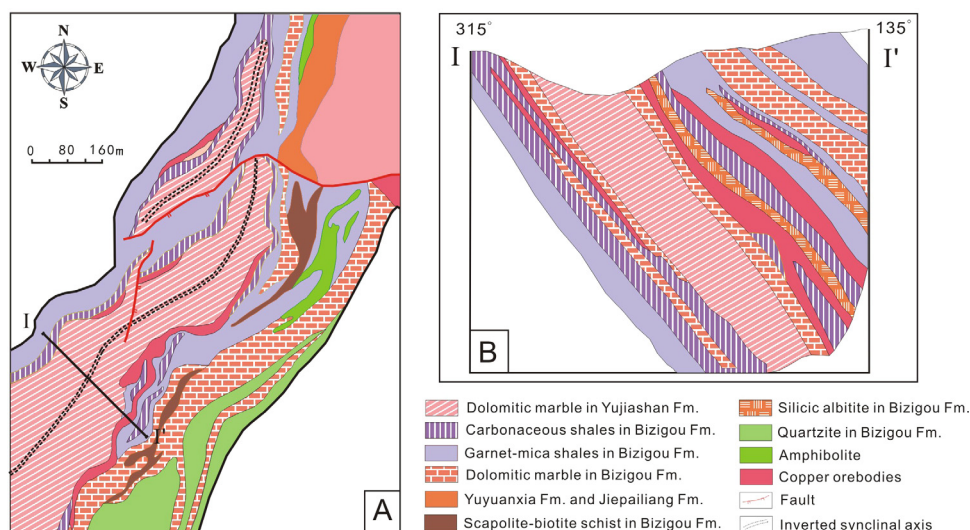Modified after Sun and Hu (1993).

1. The early mineralization stage is the major ore-forming stage. The mineralization is characterized by disseminated to veinlet (<0.5 cm wide) metal sulfides in silicic albitite and dolomitic marble. The ore minerals are mainly chalcopyrite, pyrite, and pyrrhotite with accessory chalcocite, bornite, molybdenite, cobaltite, and lesser linneite. Gangue minerals are mainly dolomite, quartz, and albite. Bedding is deformed around metal sulfide nodules due to differential compaction, suggesting the nodules were emplaced early in diagenesis (Fig. 3E). The veinlets are thin and discontinuous with irregular boundaries against the host rocks (Figs. 3E and 4C). Almost all the nodules and veinlets are aligned parallel to the stratification of silicic albitite and dolomitic marble (Fig. 3E).

2. The late stage mineralization is hosted within quartz-dolomite veins (3–20 cm wide) that are more continuous and thicker than those of the early stage (Figs. 3B, F and 4D). The vein minerals consist of chalcopyrite, pyrite, pyrrhotite quartz and dolomite. The ore veins are controlled by tectonic fractures and often cross-cut the stratigraphy of the host rocks and the early stage metal sulfide veinlets (Figs. 3B, F and 4B). The grain size of metal sulfides and gangue minerals is much coarser in the late stage veins.
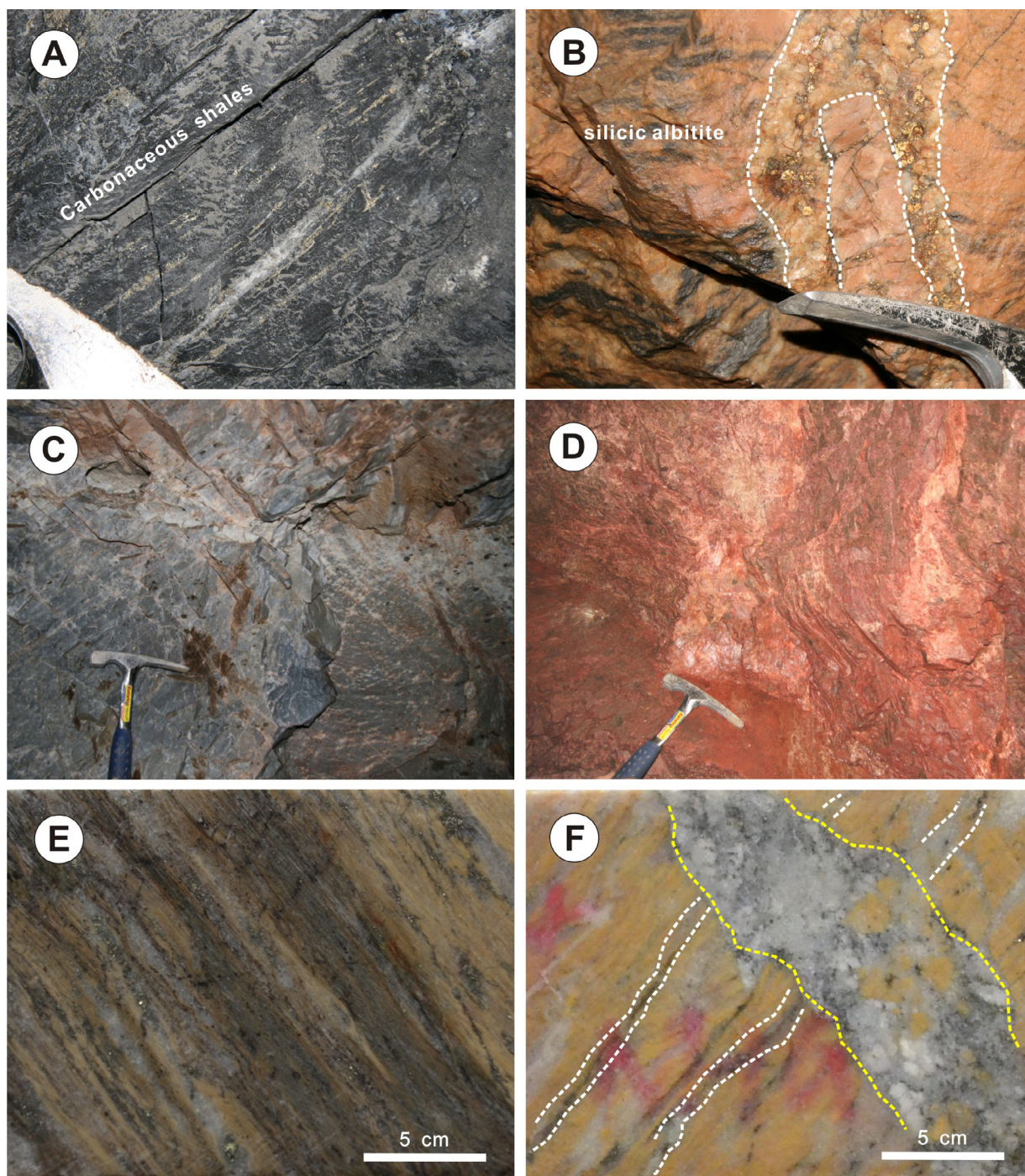
4. Analytical methods

4.1. Sampling

Eighty-five samples were collected from the No. 3 orebody and all samples were examined and described in detail. Thirty-six thin sections and 12 polished sections were examined by both transmitted and reflected light microscopes. Thirty-seven doubly polished

Fig. 2. Schematic geological map (A) and profile (B) of the Hujiayu Cu deposit. Modified after CGGCDZM (1978) and Sun and Hu (1993).
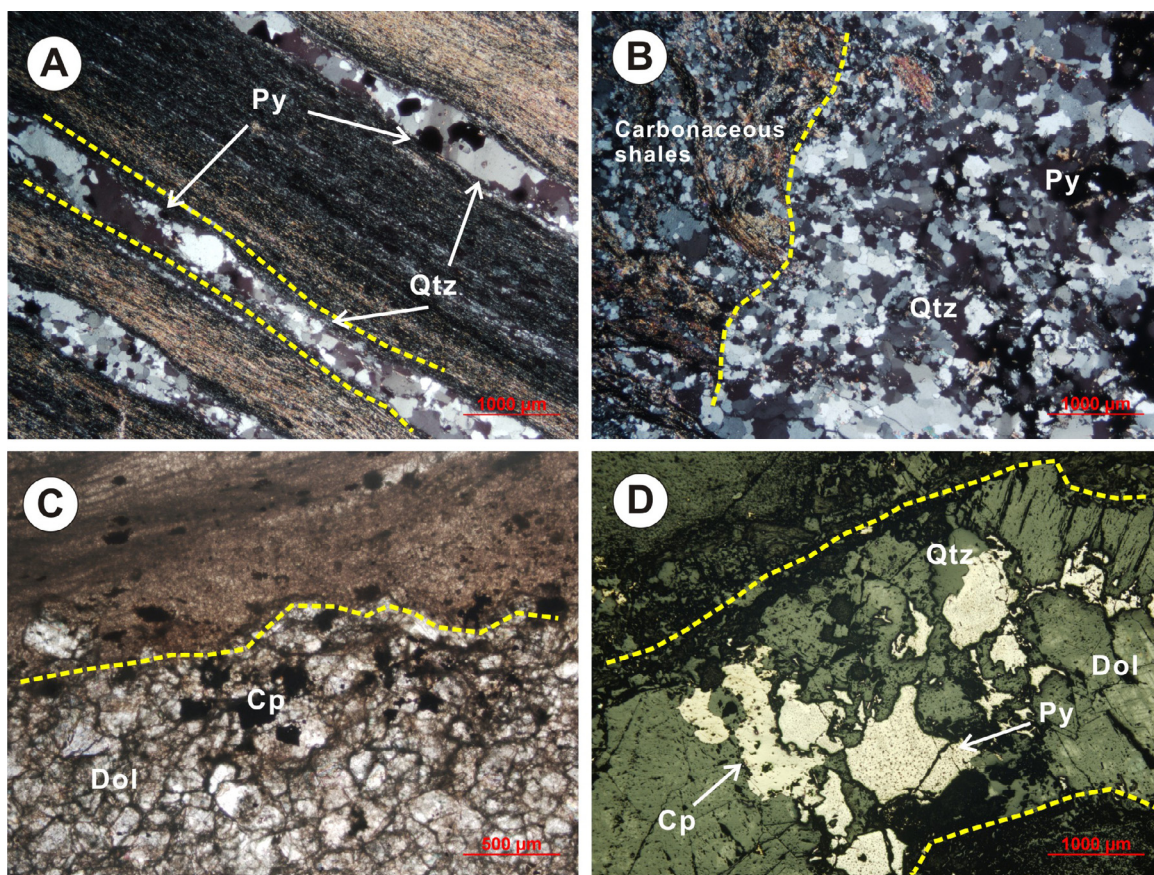
Fig. 3. Occurrence of the different stages mineralization and host rocks. (A). Thin veins mineralization in carbonaceous shales. (B). Late stage metal sulfide veins cross-cut the stratification of the silicic albitite. (C). Gray dolomitic marble in the upper parts of the Bizigou Formation. (D). Red dolomitic marble in the lower parts of the Bizigou Formation. (E). The nodules and veinlets of metal sulfides and gangue minerals in the early mineralization stage. The nodules are surrounded by locally deformed silicic albitite laminae due to differential compaction. The veinlets are thin and discontinuous and have irregular boundaries with silicic albitite. The nodules and veinlets are parallel to the stratification of silicic albitite. (F). The late stage metal sulfide veins cross-cut the early stage ore-bearing veinlets.

sections, representing the different mineralization stages, were prepared for fluid inclusion study. Microthermometric study of fluid inclusions on 22 representative doubly polished sections was conducted. To ensure that the fluid inclusions were representative of ore formation, only fluid inclusions hosted within quartz and dolomite paragenetic with metal sulfides were chosen (Chi and Xue, 2011; Jiang et al., 2013a). Fluid inclusions in these gangue minerals trapped along the same growth zone or cluster, were interpreted to represent primary ore-forming fluids (Goldstein and Reynolds, 1994).

4.2. Microthermometry

Microthermometry study was carried out on a Linkam MDS 600 Heating–Freezing System at the Key Laboratory of Mineralogy and Metallogeny, Chinese Academy of Sciences. Thermocouples were calibrated in the range of −196 °C to 600 °C using synthetic fluid inclusions. The precision of temperature measurement is ±0.1 °C between −100 °C and 25 °C; ±1 °C between 25 and 400 °C; and ±2 °C for temperature above 400 °C. The heating rate was generally 0.2–5 °C/min during the process of fluid inclusion testing, but

Fig. 4. Microphotographs of the fluid inclusion samples from the Hujiayu Cu deposit. (A) The arrangement of pyrite is parallel to the stratification of carbonaceous shales. (B) Carbonaceous shales cut by a late stage quartz-dolomite sulfide vein. (C) Dolomite–pyrite veinlet of the early stage. (D) Chalcopyrite and pyrite in the quartz-dolomite veins of the late stage. Abbreviations: Dol = dolomite; Qtz = quartz; Cp = chalcopyrite; Py = pyrite.

reduced to $0.1\,°C/min$ near the freezing point, and $0.2–0.5\,°C/min$ near the homogenization temperature to record the phase transformation process accurately.

4.3. Laser Raman microspectroscopy

Vapor and solid compositions of individual fluid inclusions were measured using the LabRam HR800 laser Raman microspectroscopy at the Institute of Geology and Geophysics, Chinese Academy of Sciences. An Ar$^+$ ion laser operating at 44 mW was used to produce an excitation wavelength of 532 nm line. The scanning range of spectra was set between 100 and 4000 cm^{-1} with an accumulation time of 10 s for each scan. The spectral resolution was 0.65 cm^{-1}. The Raman shift of a monocrystalline silicon piece was measured to be 520.7 cm^{-1} before analyzing.

4.4. Fluid inclusion references

The salinity of aqueous fluid inclusions, expressed as wt.% NaCl equiv., was estimated using the data of Bodnar (1994) for the NaCl–H$_2$O system. The salinities of halite daughter mineral-bearing inclusions were estimated using the methodology of Lecumberri-Sanchez et al. (2012) based on the temperature of bubble dissolution and homogenization temperature. Salinities of the CO$_2$-bearing inclusions were calculated using the equation given by Roedder (1984). For inclusions with eutectic temperatures less than $-21.2\,°C$, the system is approximated by H$_2$O–NaCl–CaCl$_2$, and the salinities were calculated using the equations of Chi and Ni (2007).

4.5. Carbon and oxygen isotopes

The carbonate minerals in the ores and dolomitic marble host rocks of the Bizigou Formation were collected for carbon and oxygen isotope analyses. The carbonate minerals were crushed to 60 mesh and handpicked under a binocular microscope, and then crushed to 200 mesh for isotope analyses. Carbon and oxygen isotope analyses were performed with a VG IsoPrime II mass spectrometer at the State Key Laboratory of Isotope Geochemistry in the Guangzhou Institute of Geochemistry, Chinese Academy of Sciences. Carbon dioxide was liberated from 20 mg of sample by reaction with 100% phosphoric acid in a vacuum and analyzed for O and C isotopes. Analytical uncertainties are better than $\pm0.08‰$ for $\delta^{18}O$ (reported relative to SMOW) and $\pm0.05‰$ for $\delta^{13}C$ (relative to PDB), respectively.

5. Results

5.1. Fluid inclusion petrography

5.1.1. Types of fluid inclusions

Five types of fluid inclusions have been identified based on the phases that occur at room temperature, phase transitions during total homogenization, and laser Raman spectroscopy. These five fluid inclusion types are summarized in Table 1 and described in the following.
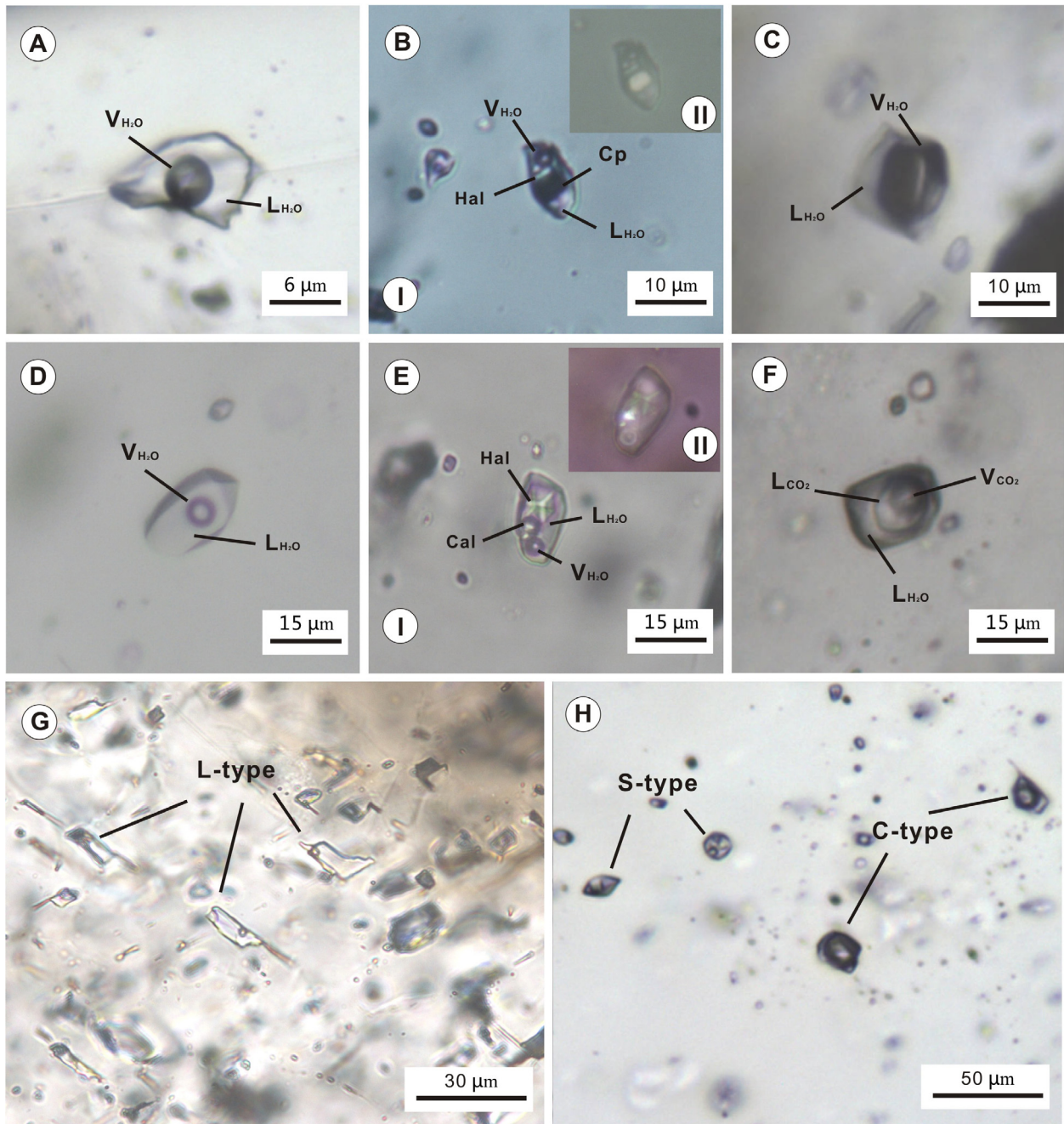
1) V-type (pure vapor or vapor-rich) inclusions: these inclusions consist of pure vapor and with occasionally <20 vol.% liquid. V-type inclusions generally range from 5 to 26 μm in diameter,
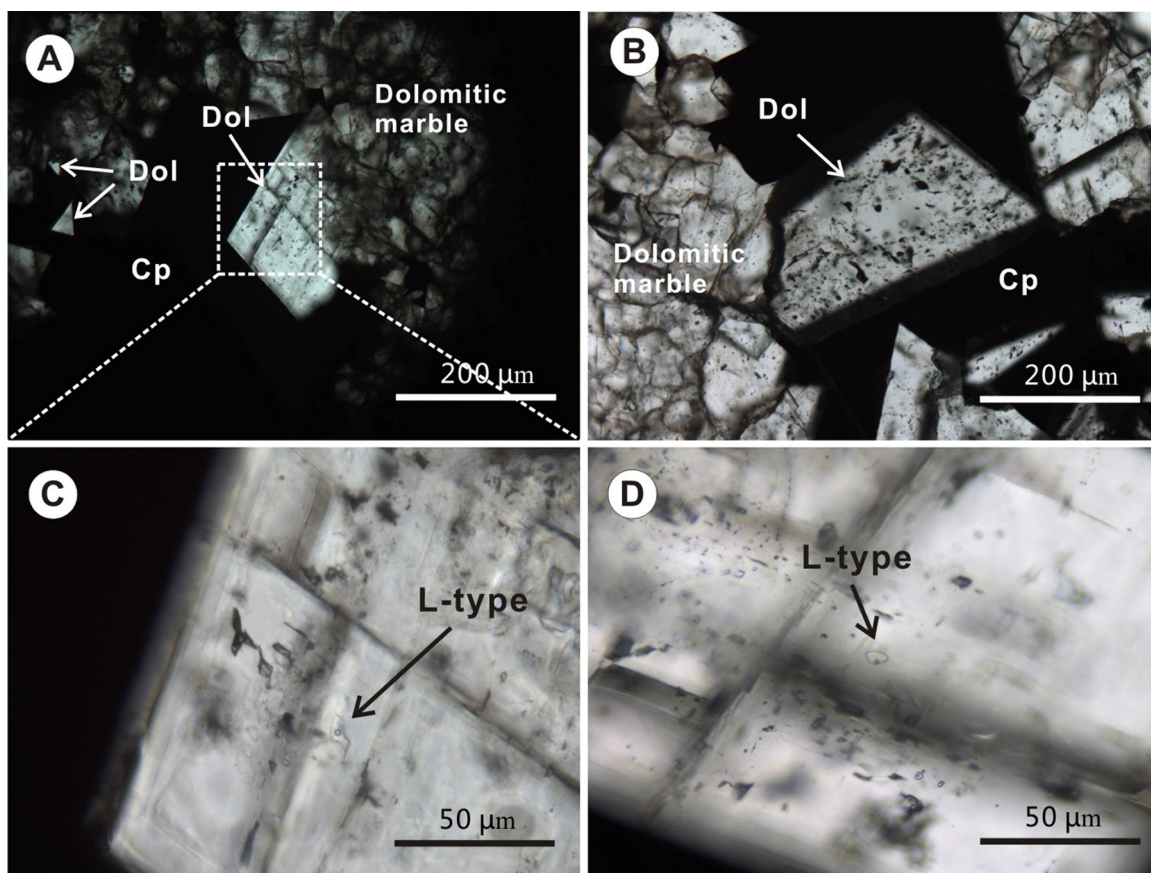
Table 1
Overview of fluid inclusion types of the Hujiayu Cu deposit.

Type	Fluid phases	Daughter minerals	Size (μm)	Vol.%	Shape	Occurrence
PC	Pure CO_2		2–25	100	Negative or elliptical	Aligned or in clusters
C	$V_{CO_2} + L_{H_2O}$ or $V_{CO_2} + L_{CO_2} + L_{H_2O}$		3–28	35–80	Negative or elliptical	Aligned or in clusters
V	V_{H_2O} or $V_{H_2O} = L_{H_2O}$		5–26	>80	Elliptical	Randomly distributed
L	$V_{H_2O} + L_{H_2O}$		1–20	<35	Irregular, negative	Randomly distributed or in clusters
S	$V_{H_2O} + L_{H_2O}$	Halite, sylvite, calcite, chalcopyrite, unidentified	2–29	10–30	Negative, elliptical	Randomly distributed, aligned, or in clusters

Abbreviations: V_{CO_2} = CO_2 vapor; L_{CO_2} = CO_2 liquid; V_{H_2O} = H_2O vapor; L_{H_2O} = H_2O liquid; vol.% = volume percentage of the vapor phase.

Fig. 5. Microphotographs of the fluid inclusions in the Hujiayu Cu deposit. (A) Early stage L-type inclusion with V_{H_2O} and L_{H_2O}. (B) Early stage S-type inclusion with halite and chalcopyrite daughter minerals. Microphotographs I and II were taken using plane-polarized light and reflected light, respectively. (C) Early stage V-type inclusion with V_{H_2O} and L_{H_2O}. (D) Late stage L-type inclusion with V_{H_2O} and L_{H_2O}. (E) Late stage S-type inclusion with halite and calcite daughter minerals. Microphotographs I and II were taken using are plane-polarized light and cross-polarized light, respectively. (F) Late stage C-type inclusion with V_{CO_2}, L_{CO_2}, and L_{H_2O}. (G) Early stage L-type inclusions in dolomite occur as random distribution. (H) Late stage C-type and S-type inclusions. Abbreviations: V_{CO_2} = CO_2 vapor; L_{CO_2} = CO_2 liquid; V_{H_2O} = H_2O vapor; L_{H_2O} = H_2O liquid; Hal = halite; Cal = calcite; Cp = chalcopyrite.

Fig. 6. Microphotographs showing the features of syn-ore dolomite and fluid inclusions in them. (A) and (B) show the presence of dolomite grains inside early stage chalcopyrite. The grains show a straight contact with chalcopyrite, indicating that dolomite and chalcopyrite are intergrown. (C) and (D) show the L-type inclusions in the dolomite of the (A) and (B), respectively. Abbreviations: Dol = dolomite; Cp = chalcopyrite.

and are mainly elliptical in shape (Fig. 5C). They are generally distributed randomly and sometimes occur with S-type inclusions.

2) C-type (CO_2–H_2O) inclusions: these inclusions consist of two (liquid H_2O + CO_2-rich supercritical fluid) or three phases (vapor CO_2 + liquid CO_2 + liquid H_2O) at room temperature. C-type inclusions commonly occur in lines or clusters, mainly as negative crystals and are elliptical in shape. These fluid inclusions are commonly 3–28 μm in diameter, and the carbonic phases occupy 35–80 vol.% (Fig. 5F).

3) PC-type (pure CO_2) inclusions: they are CO_2-only inclusions. The inclusions are generally 2–25 μm in diameter and occur mainly as negative crystals and are elliptical in shape. PC-type inclusions usually occur in lines or clusters (Fig. 5H).

4) L-type (liquid-rich) inclusions: these inclusions consist of liquid and < 35% vapor. They are 1–20 μm in size and have either irregular or negative crystal shapes (Fig. 5A and D). L-type inclusions are dominated by H_2O and occur in clusters or as random distributions.

5) S-type (daughter mineral-bearing) inclusions: the S-type inclusions mostly occur in negative crystal and elliptical shapes with vapor phases occupying 10–30 vol.%. They range from 2 to 29 μm in diameter and contain abundant daughter minerals such as halite, sylvite, calcite, chalcopyrite (Fig. 5B, E, and H), and other unidentified daughter minerals. Halite is the dominant daughter mineral in the S-type inclusions. These inclusions occur in random distributions, lines, and clusters (Fig. 5H).

5.1.2. Occurrence and temporal relationship of fluid inclusions

Systematic petrographic observation is very important to infer the relative timing of fluid entrapment and to study the implications of fluid migration (Goldstein and Reynolds, 1994; Ulrich and Heinrich, 2001). Our study shows that fluid inclusions in the early and late stages of paragenesis are significantly different in fluid inclusion type, assemblage, and composition.

The quartz-dolomite sulfide veinlets in the early stage are generally very thin (<0.5 cm) and contain fewer inclusions than the late stage veins. Dolomite and quartz that direct contact with chalcopyrite (Fig. 6A and B) were chosen for fluid inclusion study. The types of fluid inclusions from the early stage mineralization include mainly L-type, S-type, and lesser V-type. Neither C-type nor PC-type inclusion has been found in this mineralization stage. The S-type and V-type inclusions coexist in quartz and dolomite, indicating that the two types of inclusions may have been trapped simultaneously. The daughter minerals in these S-type inclusions are mainly halite with minor chalcopyrite (Fig. 5B).

In the late mineralization stage, ore-bearing quartz-dolomite sulfide veins are relatively thicker (3–20 cm wide) than those in the early stage and contain abundant inclusions of larger size. PC and C-type inclusions are typically the dominant types in this stage and they occur both in lines and clusters. Gangue minerals that contain C-type inclusions also commonly contain S-type inclusions. The coexistence of these two types of inclusions suggests that the fluid may have experienced phase separation (Fig. 5H). Halite and calcite daughter minerals coexist in the S-type

Table 2
Microthermometric data of fluid inclusions in the Hujiayu Cu deposit.

Stage	Type	Number	T_{m,CO_2} (°C)	Ti (°C)	$T_{m,ice}$ (°C)	$T_{m,cla}$ (°C)	Th_{CO_2} (°C)	Tv (°C)	$T_{m,hal}$ (°C)	Th (°C)	Salinity (wt.% NaCl)
Early Stage	L	118		−61.8 to −47.0	−36.0 to −3.1			102–350		102–350	5.1–27.5
	S	56						103–277	120–350	120–350	28.8–42.1
	V	11		−59.1 to −48.5	−8.3 to −1.6					185–399	2.7–12.5
Late Stage	PC	24	−60.9 to −56.6				−0.1 to 17.0				
	C	25	−61.2 to −56.6			−9.5 to −0.4	−2.3 to 17.9			239–459	15.92–20.46
	L	55		−21.2 to −18.9	−21.2 to −3.1			123–477		123–477	4.2–23.18
	S	41						138–325	215–515	215–515	33.4–53.0

Abbreviations: T_{m,CO_2} (°C) = melting temperature of CO_2; Ti (°C) = first ice-melting temperature; $T_{m,ice}$ (°C): temperature of ice point; $T_{m,cla}$ (°C) = melting temperature of CO_2–H_2O clathrate; Th_{CO_2} (°C) = partial homogenization temperature of CO_2; Tv (°C) = bubble disappearance temperature; $T_{m,hal}$ (°C) = melting temperature of halite; Th (°C) = final homogenization temperature.
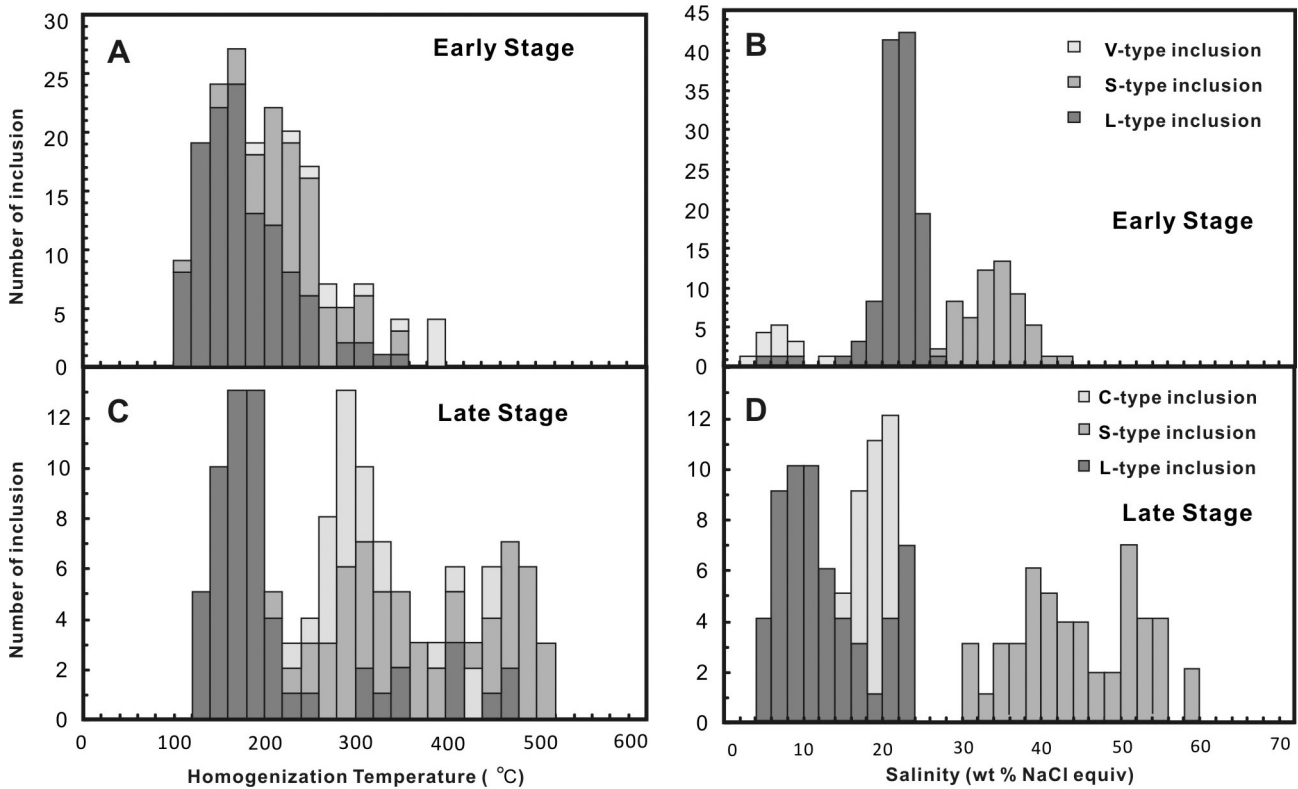

Fig. 7. Histograms of salinities and homogenization temperatures of fluid inclusions in both the early stage and the late stage.

inclusions (Fig. 5E). L-type inclusions are also common in the late stage mineralization.

5.2. Microthermometric results

The results of the microthermometric analyses of the fluid inclusions are summarized in Table 2 and Figs. 7 and 8.

PC-type inclusions contain liquid CO_2 and vapor bubbles during cooling runs. The melting temperatures for solid CO_2 range from −60.9 °C to −56.6 °C, and the homogenization temperatures of CO_2 to the liquid phase vary from −0.1 °C to 17 °C (Table 2; Fig. 8).

In C-type inclusions, melting of solid CO_2 occurs at temperatures from −61.2 °C to −56.6 °C. The melting temperatures are somewhat lower than the triple point for pure CO_2 (−56.6 °C), suggesting the presence of other minor gases. However, these gases were not detected in our laser Raman spectroscopy analyses (Fig. 10B). The melting temperatures of CO_2 clathrate vary from −9.5 °C to −0.4 °C, indicating that the salinities of these inclusions range from 15.92 to 20.46 wt.% NaCl equiv. (Fig. 7D). CO_2 is only homogenizing to liquid,
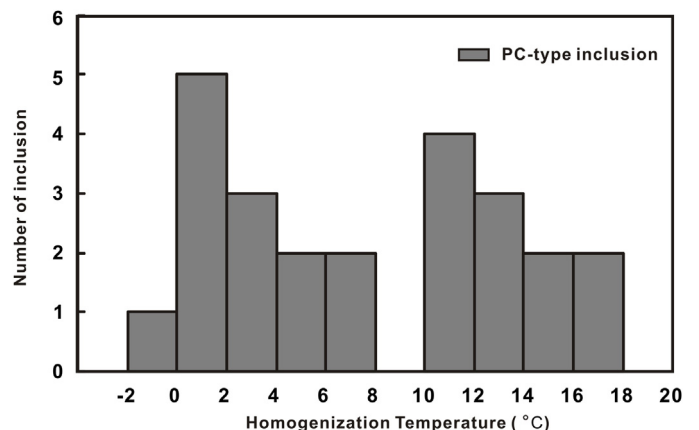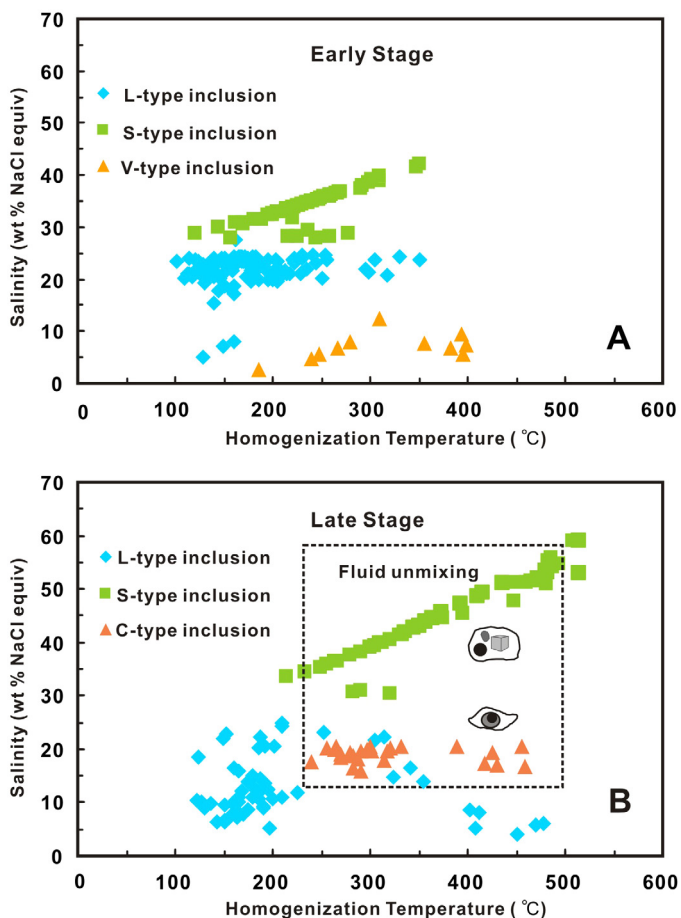

Fig. 8. Histogram showing partial homogenization of PC-type inclusions to liquid.

Fig. 9. Homogenization temperatures versus salinities of fluid inclusions in both early stage (A) and late stage (B). Some coexisting S-type and V-type inclusions in Fig. 7A, have similar homogenization temperatures and show fearures of unmixing. In Fig. 7B, S-type and C-type inclusions show the typical microthermometric behaviors of unmixing assemblage, indicating that the escape of CO_2 led to the discharge of Cu in the late stage.

with corresponding partial homogenization temperatures ranging from −2.3 °C to 17.9 °C. Total homogenization temperatures show a wide range of variation from 239 °C to 459 °C, with two peaks at 239–332 °C and 389–459 °C, respectively (Fig. 7C).

In the early stage mineralization, S-type inclusions exhibit two different ways of homogenization. Usually they homogenize by halite disappearance and rarely by bubble disappearance. The homogenization temperatures of these inclusions range from 120 °C to 350 °C, with corresponding salinities of 28.8–42.1 wt.% NaCl equiv. (Fig. 7A and B). In the late stage mineralization, S-type inclusions homogenize at temperatures between 215 °C and 515 °C, with corresponding salinities of 33.4–53 wt.% NaCl equiv. (Fig. 7C and D). Almost all S-type inclusions of the late stage homogenize by halite disappearance, except three inclusions which homogenized by bubble disappearance.

For L-type inclusions of the early stage mineralization, the first melting temperatures range from −61.8 °C to −47 °C (Table 2). Given that most of the data focus on −52 °C, we assume that the fluids are H_2O–NaCl–$CaCl_2$ systems to estimate salinity (Oakes et al., 1990; Chi and Ni, 2007). Ice melting temperatures of the L-type inclusions vary from −36 °C to −3.1 °C, with corresponding salinities of 5.1–27.5 wt.% NaCl equiv. The total homogenization to liquid occurs at temperatures ranging from 102 °C to 350 °C, with most between 102 °C and 255 °C. The first melting temperatures of L-type inclusions of the late stage range from −21.2 °C to −18.9 °C, indicating that the fluid is NaCl–H_2O system. Ice melting temperatures of

these inclusions range from −21.2 °C to −3.1 °C, with corresponding salinities of 4.2–23.1 wt.% NaCl equiv. All homogenization temperatures range from 123 °C to 477 °C (Fig. 7C).

V-type inclusions show consistent microthermometric behavior by homogenizing to vapor. The first melting temperatures of V-type inclusions from the early stage range from −48.5 °C to −59.1 °C, and the ice melting temperatures of these inclusions range from −8.3 °C to −1.6 °C. The homogenization of V-type inclusions occur at temperatures from 185 °C to 399 °C, exhibiting a wide variation. The salinities of these inclusions range from 2.7 to 12.5 wt.% NaCl equiv.

5.3. Laser Raman spectroscopy analysis

Representative inclusions were measured by laser Raman spectroscopy. The vapor phase compositions of V-type, S-type, and L-type inclusions were primarily water (Fig. 10A). The PC-type and C-type inclusions showed evident characteristic peaks for CO_2 (1279 and 1384 cm^{-1}; Fig. 10B). Chalcopyrite (291 cm^{-1}; Fig. 10C) and calcite (1083 cm^{-1}; Fig. 10D) daughter minerals were recognized in the S-type inclusions.

5.4. Carbon and oxygen isotopes

Carbon and oxygen isotope data from this study and those in the literature are presented in Table 3. The dolomitic marble from the Bizigou Formation have $\delta^{13}C_{V-PDB}$ and $\delta^{18}O_{V-SMOW}$ varying from 0.29‰ to 0.48‰ and 22.55‰ to 23.01‰, respectively. The $\delta^{13}C_{V-PDB}$ and $\delta^{18}O_{V-SMOW}$ values of mineralized carbonates in the early stage vary from −4.09‰ to −1.53‰ and 13.09‰ to 14.55‰, respectively. The mineralized carbonates in the late stage have $\delta^{13}C_{V-PDB}$ and $\delta^{18}O_{V-SMOW}$ varying from −10.5‰ to −1.18‰ and 13.80‰ to 15.29‰, respectively.
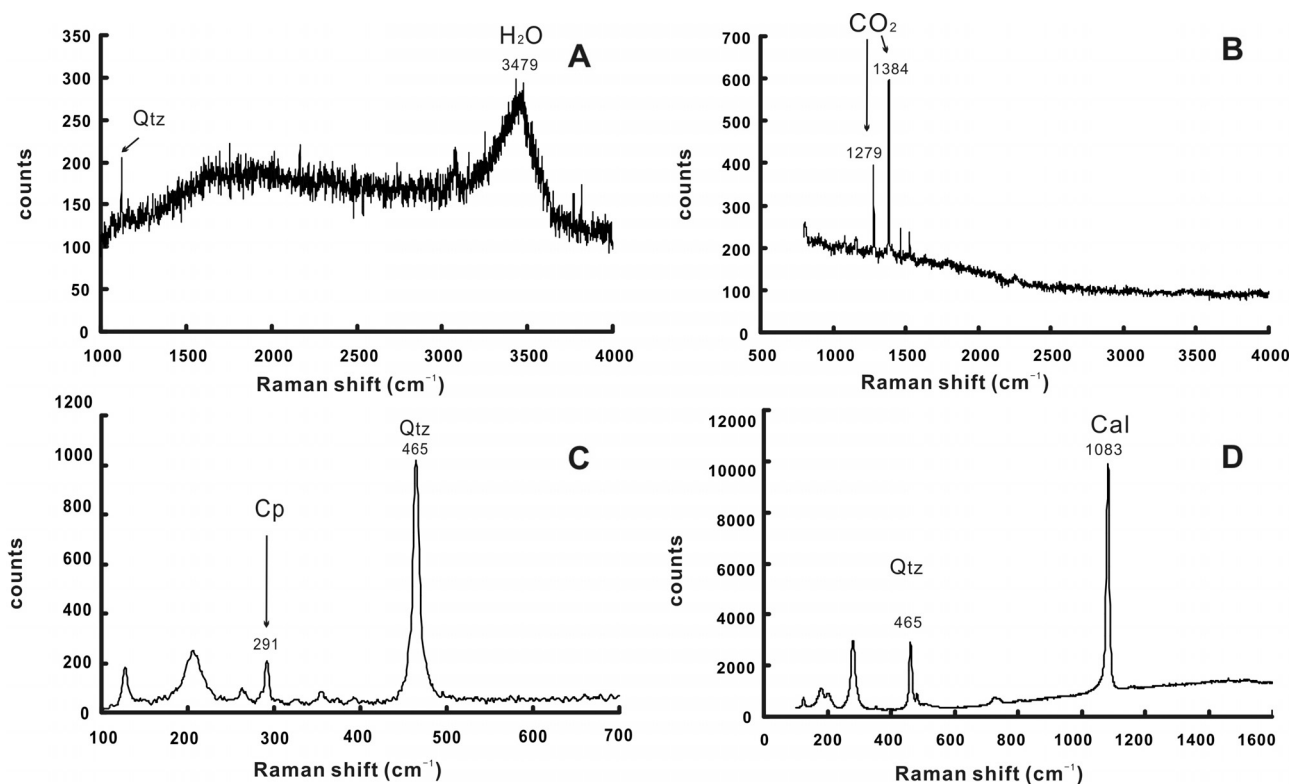
6. Discussions

6.1. Composition and characteristics of ore-forming fluids

6.1.1. High salinity fluids

In hydrothermal deposits, high salinity fluids often play a very important role in metal transport (Roedder, 1971; Holland, 1972; Crerar and Barnes, 1976; Li et al., 2009; Huston et al., 2010; Zajacz et al., 2011; Seo and Heinrich, 2013). Copper-chloride-brine is considered to be the main ore-forming fluid for sediment-hosted stratiform Cu deposits (Brown, 2005; Cailteux et al., 2005; Hitzman et al., 2005).

As shown in the salinity-total homogenization temperature diagrams (Fig. 9), most of the fluid inclusions in the Hujiayu deposit have relatively high salinities. The fluid inclusions of the early stage have salinities that mainly vary from 22 to 40 wt.% NaCl equiv. (Figs. 7B and 9A). The L-type inclusions of the early stage and the C-type inclusions of the late stage have highly variable temperatures, but similar salinities range from 15 to 25 wt.% NaCl equiv. (Fig. 7B and D). The common occurrence of S-type inclusions, in particular, represents a high saline environment.

Study on the silicic albitite showed that it was formed in an evaporitic environment (Wei et al., 1984). A mechanism for massive albite formation is the reaction between detrital feldspar and dissolved evaporates (Land and Milliken, 1981). The reaction can also release typical sedimentary basin brines (containing sodium, calcium, and chloride), consistent with the compositions (primarily H_2O–NaCl–$CaCl_2$ systems) of the early ore-forming fluid at Hujiayu. This is also consistent with other sediment-hosted stratiform Cu deposits, which are commonly associated with evaporates units that are the main source of high salinity fluids (Brown, 1997). Furthermore, scapolite phenocrysts are widespread in the dolomitic

Fig. 10. The laser Raman spectra of fluid inclusions. (A) H_2O-spectra of the liquid in a L-type inclusion. (B) CO_2-spectra of the liquid in a C-type inclusion. (C) Chalcopyrite-spectra of the daughter mineral in a S-type inclusion. (D) Calcite-spectra of the daughter mineral in a S-type inclusion. Abbreviations: Cal = calcite; Cp = chalcopyrite; Qtz = quartz.

Table 3
Carbon and oxygen isotopes from the Hujiayu Cu deposit. $\delta^{18}O_{V\text{-}SMOW}(‰) = 1.03091 \times \delta^{18}O_{V\text{-}PDB}(‰) + 30.91$, according to Coplen et al. (1983).

Sample	$\delta^{13}C_{VPDB}$	$\delta^{18}O_{VPDB}$	$\delta^{18}O_{V\text{-}SMOW}$	Source
Dolomitic marble (Bizigou Formation)				
D209B-80	0.48	−7.66	23.01	This study
809-640-3	0.39	−7.86	22.80	This study
809-640-2	0.29	−7.97	22.70	This study
809-640-1	0.29	−8.11	22.55	This study
Dolomitic marble (Yujiashan Formation)				
NHG-ZD240-4XC-B7	−1.2	−12.50	17.97	Huang et al. (2013)
NHG-ZD240-4XC-B6	−1.0	−13.90	16.53	Huang et al. (2013)
NHG-240ZD-CM2-B4	0.7	−9.20	21.38	Huang et al. (2013)
NHG-240ZD-CM96-B3	−0.6	−11.30	19.21	Huang et al. (2013)
Mineralized carbonate (early stage)				
HUK-CC-1	−2.01	−16.33	14.07	This study
D401-200	−3.97	−15.87	14.55	This study
13HJ3-3	−4.09	−16.60	13.80	This study
HUK439-04-1	−1.78	−17.29	13.09	This study
HUK439-04-2	−1.53	−16.83	13.56	This study
Mineralized carbonate (late stage)				
HUK240Z5-1-1	−2.86	−15.16	15.28	This study
HUK240Z5-1-2	−1.18	−15.15	15.29	This study
HUK	−5.91	−15.57	14.86	This study
D301-70	−10.50	−15.92	14.50	This study
D301-112	−2.73	−16.15	14.26	This study
D301-115	−4.39	−16.21	14.19	This study
D401-65	−8.60	−15.79	14.63	This study
Mineralized carbonate of the Hujiayu Cu deposit				
NHG-240ZD-CM94-B10	−3.9	−17.3	13.03	Huang et al. (2013)
NHG-240ZD-CM94-B10′	−2.2	−17.3	13.03	Huang et al. (2013)
NHG-240ZD-CM96-B1	−0.9	−16.8	13.54	Huang et al. (2013)
NHG-240ZD-CM96-B1′	−1.1	−16.4	13.95	Huang et al. (2013)
NHG-240ZD-CM94-B14	−0.2	−16.9	13.44	Huang et al. (2013)
NHG-240ZD-CM96-B4	−2.8	−16	14.37	Huang et al. (2013)
NHG-240ZD-CM94-B2	−0.4	−17	13.34	Huang et al. (2013)

marble of the Zhongtiao Group and scapolite–biotite schist occurs at the bottom of the Bizigou Formation (Sun and Hu, 1993; Sun et al., 1995). The occurrence of scapolite is usually believed to be closely associated with the migration of high salinity fluids (Oliver et al., 1994; Pollard, 2001; Moore, 2010). This indicates that the carbonate rocks of the Bizigou Formation may have been affected by chlorine-rich fluids in the early stages of formation. The EMPA analysis of scapolite in the scapolite–biotite schist shows that the content of Cl is up to 2.5–3.0% (Sun and Hu, 1993). Therefore, we infer that the ore-forming fluids extracted Cl from the evaporite and scapolite–biotite schist. Chlorine-rich fluid is the main carrier of Cu in the Hujiayu copper deposit. The salinities of S-type inclusions of the late stage are significantly higher than those in the early stage (Fig. 7B and D). This can be explained by significant fluid unmixing in the late stage.

6.1.2. Fluid unmixing and the role of CO_2

In the early mineralization stage, the coexistence of S-type and V-type inclusions can be found in some quartz veinlets. Given that the two types of inclusions have approximately identical homogenization temperature ranges (Fig. 7A), but homogenize into different phases, it can be confirmed that unmixing occurred locally at this stage (Fig. 9A). This unmixing assemblage has relatively higher homogenization temperatures than the other inclusions of the early stage. Previous studies have shown that the Cu content of amphibolite near the orebodies is much lower than the amphibolite far away from the orebodies, which indicates that the amphibolite is a source of copper for the ore-forming fluids (Cen et al., 1993). Hitzman et al. (2010) also propose that igneous activity can participate in the mineralization of sediment-hosted stratiform copper deposits. Therefore, the unmixing assemblage in the early stage may represent the presence of magmatic fluids. In the late stage mineralization, fluid unmixing can easily be discerned by the coexistence of PC-type, C-type, and S-type inclusions (Fig. 5H). The microthermometric results further corroborate the existence of fluid unmixing (Fig. 9B). The unmixing fluids are composed of a CO_2-rich facies (PC type and C type inclusions) and a high salinity facies (S-type inclusions). Indeed, calcite daughter minerals are commonly observed in the S-type inclusions which represent the high salinity end member of the unmixing fluids. The solubility of calcite in hydrothermal system increases with decreasing temperature, but also decreases with decreasing pressure (Holland and Malinin, 1979; Zheng, 1990). Thus, simple cooling alone cannot lead to the deposition of calcite. Degassing of CO_2 is an important way of calcite precipitation (Zheng and Chen, 2000), which can decrease the solubility of calcite. Therefore, the escape of CO_2 from solutions can change the physical and chemical conditions of the remaining fluids and promote the precipitation of Cu (Lowenstern, 2001; Robb, 2009). The source of CO_2 in the fluids is believed to be closely related to regional metamorphism during the Zhongtiao movement.

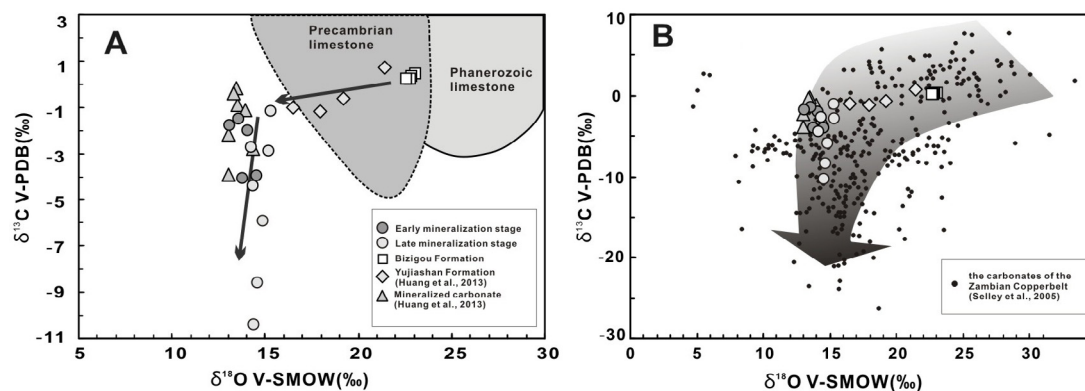### 6.1.3. Composition and homogenization temperature of the fluid system

The L-type inclusions from the different stages exhibit distinct microthermometric behaviors under cooling. For example, first melting temperatures for L-type inclusions of the early stage vary from −61.8 °C to −47 °C, suggesting complex compositions of the fluid system. We argue that the fluids are H_2O–$NaCl$–$CaCl_2$ systems (Oakes et al., 1990; Chi and Ni, 2007) derived from evaporates, red dolostone, siltstone, and volcanic rocks (Hitzman et al., 2005, 2010). In contrast with the early stage, the L-type inclusions in the late stage are representative of a relatively simple H_2O–$NaCl$ system. The striking difference of fluid systems for the early and late mineralization stage suggests that the two stages of mineralization are of different origin.

The microthermometric data of fluid inclusions can efficiently reflect the physico-chemical conditions of ore-forming fluids in different mineralization stages (Fig. 9). The homogenization temperatures of fluid inclusions in the early stage show a wide range of variation from 102 °C to 399 °C, with mostly between 120 °C and 280 °C. The homogenization temperatures of the total fluid inclusions range from 123 °C to 515 °C, but the homogenization temperatures of C-type and S-type inclusions representing extensive unmixing vary from 240 °C to 480 °C (Fig. 9B). This is consistent with the temperature of low-grade greenschist facies to high-grade greenschist facies metamorphism. The lower homogenization temperatures of some L-type inclusions may result from the progressive cooling of fluids and the incorporation of meteoric water in the late mineralization stage. Cen (1993) investigated the characteristics of H and O isotopes of the fluid inclusions in the Hujiayu Cu deposit. The results show that the ore-forming fluids consist of magmatic, metamorphic, and meteoric water. El Desouky et al. (2009) studied the ore-forming fluids of two main Cu–Co sulfide stages in the Katanga Copperbelt of the Central African Copper Belt. The first stage produced early diagenetic stratiform mineralization related to a moderate temperature (115–220 °C) and moderate salinity (11.3–20.9 wt.% NaCl equiv.) fluid (El Desouky et al., 2009). The second stage producing late syn-orogenic Cu mineralization is related to a high temperature (270–385 °C) and high salinity (35–45.5 wt.% NaCl equiv.) fluid (El Desouky et al., 2009). The microthermometric trend of fluid inclusions in the Katanga Copperbelt is comparable with the trend observed at the Hujiayu Cu deposit.

6.2. Interpretation of carbon and oxygen isotopes

The C–O isotope compositions diagram (Fig. 11A) shows an elongated data distribution for the early and late stage mineralized carbonates. For the early stage samples, oxygen isotope values have a relatively narrow range of variation (13.09–14.55‰) but carbon isotope values have a considerably wider range of variation (−10.5‰ to −1.18‰). Carbon isotope fractionation between mineral-fluid does not depend on temperature significantly (O'Neil et al., 1969). Thus, we believe that the mixing of fluids with different carbon isotope compositions resulted in the observed variation of carbon isotope compositions in the mineralized carbonates. This inference can be explained by ore-forming model of sediment-hosted stratiform Cu deposits (Hitzman et al., 2010). In this type of deposit, reductants within the rocks overlying the red beds are essential for the precipitation of Cu sulfides (Hitzman et al., 2010). The reductants act as a chemical trap for the reduction of oxidized copper-bearing brines and discharge of copper (Brown, 1992; Hitzman et al., 2010). The reducing rocks are carbonaceous shales in most sediment-hosted stratiform Cu deposits (Hitzman et al., 2005; Zhao et al., 2012b). In the Hujiayu Cu deposit, carbonaceous shales are ubiquitous in the strata between the top of the Bizigou Formation and the bottom of the Yujiashan Formation. Locally mineralization can be observed in the carbonaceous shales (Fig. 2B). The interaction between the oxidized Cu-bearing brines and reduced carbonaceous shales would have resulted in the oxidation of organic matter (Selley et al., 2005; El Desouky et al., 2010), which may be the main reason for the significant variation of carbon isotope values.

The late stage mineralization overprints the early mineralization, and thus the carbon and oxygen isotope values of the mineralized carbonates in the late stage veins have distribution characteristics similar to those in the early stage. However, two late stage mineralized carbonate samples have the carbon isotope values of −8.6‰ and −10.5‰, respectively (Fig. 11A). This shows that the carbon isotope values of the late stage mineralized carbonates have a wider range of variation than those in the early stage.

Fig. 11. Carbon and Oxygen isotope compositions. (A) Carbon and Oxygen isotope data for dolomites of host strata and carbonate minerals in ore veins from the Hujiayu Cu deposit. Carbon and Oxygen isotope values decrease from the marble of the Bizigou Formation and the Yujiashan Formation to ore veins of the Hujiayu mine gradually. (B) The $\delta^{13}C$ and $\delta^{18}O$ data from 369 carbonate samples (whole rock, veins, and evaporate nodules) from 10 deposits in the Zambian Copperbelt compiled by Selley et al. (2005). The trends of $\delta^{13}C$ and $\delta^{18}O$ variations are similar to those of the Hujiayu deposit. The variation of Precambrian and Phanerozoic limestone is in accordance to those reported by Bell and Simonetti (2010).

The fluid inclusion study indicates that CO_2 degassing from hydrothermal solutions is common in the late stage, so the heavy carbon isotope fractionating to CO_2 may produce more negative carbon isotope values in the late stage mineralized carbonates (Zheng and Chen, 2000).

In contrast with the mineralized carbonates, the carbon and oxygen isotope values of dolomitic marble in the Bizigou Formation exhibit a narrower range of variation (Fig. 11A). This indicates that these rocks are derived from marine carbonate. Huang et al. (2013) analyzed the C and O isotope values of the mineralized carbonate veins in the Hujiayu Cu deposit and the marble in the Yujiashan Formation. The data of mineralized carbonate veins are consistent with the data of this study, but the data of the Yujiashan Formation are different from those data of the Bizigou Formation (Fig. 11A). Combining the data of Huang et al. (2013) with this study, the C and O isotope values show a gradually decrease from the unmineralized carbonates of the Bizigou Formation to the mineralized carbonates within the orebodies of Hujiayu. Carbon and oxygen isotopic data from 369 carbonate samples (whole rock, veins, and evaporate nodules) of 10 deposits in the Zambian Copper Belt were compiled by Selley et al. (2005). The $\delta^{13}C$ and $\delta^{18}O$ values shift from the Neoproterozoic marine carbonates in the unaltered sedimentary carbonates toward the hydrothermal carbonates sampled within or close to the orebodies (Fig. 11B). The trend of C and O isotope variations in the Hujiayu deposit is quite similar to those reported by Selley et al. (2005) (Fig. 11B).

6.3. Mechanism of fluid mineralization

The Hujiayu copper deposit experienced two mineralization stages, which is supported by many studies of ore geology and geochronology (CGGCDZM, 1978; Sun and Ge, 1990; Sun and Hu, 1993; Zhang, 2012). It is commonly accepted that the late stage mineralization is closely associated with the regional metamorphism during the Zhongtiao movement (1.9 Ga) (CGGCDZM, 1978; Sun and Ge, 1990; Sun and Hu, 1993; Zhang, 2012). However, the mechanism of early stage mineralization has been contentious. Sun and Ge (1990) proposed that the "Hu-Bi type" Cu deposits are hydrothermal-exhalation sedimentary deposits (similar to SEDEX). Silicic albitite is regarded as exhalative sedimentary rock. However, the economic metals of SEDEX-type deposits are mainly Pb and Zn, and lack Cu (Goodfellow and Lydon, 2007; Pirajno, 2009; Leach et al., 2010). Many researchers believe that the "Hu-Bi type" Cu deposits are sedimentary strata-bound-reformation deposits (CGGCDZM, 1978; Sun and Hu, 1993; Zhang, 2012). However,

studies that support this model lack substantial fluid inclusion data to constrain hydrothermal mineralization and they ignore roles of red beds in the lower segment of the Bizigou Formation. The oxidized red beds are a key component for the formation of sediment-hosted stratiform Cu deposits (Hitzman et al., 2010). The sedimentation of the Bizigou Formation started from 2.06 Ga (Sun and Hu, 1993), subsequent to the Great Oxidation Event (GOE) (2.4–2.06 Ga, Melezhik et al., 1999).

Based on the ore geology, fluid inclusion data and C—O isotopic analyses, we propose the following model for the early stage hydrothermal mineralization in the Hujiayu Cu deposit. High saline brines were released by the reaction between detrital feldspar and dissolved evaporates. The brines leached copper and other metals through the red-bed and formed oxidized Cu-chloride brines. As the Cu-bearing fluids migrated upwards along fractures and encountered organic-rich reducing carbonaceous shales, Cu was discharged in the form of sulfides. The basic intrusion at the bottom of the Bizigou Formation may also provide Cu and heat for the ore-forming fluids. Late stage mineralization is mainly formed by metamorphic hydrothermal solutions, which is closely associated with "Zhongtiao" movement. The discharge of Cu is most likely caused by CO_2 escaping from metamorphic hydrothermal solutions.

7. Conclusions

(1) The ore-forming fluids of the early mineralization stage are mainly characterized by high salinity (22–40 wt.% NaCl equiv.) and moderate temperature (120–280 °C). The ore-forming fluids of the late mineralization stage, are characterized by CO_2-rich and high salinity and high temperature, and experienced extensively phase separation at the temperatures of 240–480 °C. The compositions of the main ore-forming fluids in the early and late stages are basinal brines and metamorphic hydrothermal solutions, respectively.

(2) Carbon and oxygen isotope compositions of the ore-forming fluids of the early stage show that the fluids may have exchanged carbon isotope with the organic-rich carbonaceous shales. In the late mineralization stage, both degassing of CO_2 and isotopic exchange with organic carbon resulted in the more negative $\delta^{13}C_{V-PDB}$ values of the mineralized carbonates.

(3) Early stage mineralization of the Hujiayu Cu deposit may occur via interaction of oxidized Cu-bearing brines from the underlying red beds with the upper reducing carbonaceous shales. Late

stage mineralization at the Hujiayu deposit is likely related to CO_2 escaping from metamorphic hydrothermal solutions.

Acknowledgements

References

Bai, J., 1997. Precambrian crustal evolution of the Zhongtiao Mountains. Earth Sci. Front. 4, 281–289 (in Chinese with English abstract).

Bell, K., Simonetti, A., 2010. Source of parental melts to carbonatites – critical isotopic constraints. Mineral. Petrol. 98, 77–89.

Bodnar, R.J., 1994. Synthetic fluid inclusions: XII. The system H_2O–NaCl. Experimental determination of the halite liquidus and isochores for a 40 wt% NaCl solution. Geochim. Cosmochim. Acta 58, 1053–1063.

Brown, A.C., 2005. Refinements for footwall red-bed diagenesis in the sediment-hosted stratiform copper deposits model. Econ. Geol. 100, 765–771.

Brown, A.C., 1997. World-class sediment-hosted stratiform copper deposits: characteristics, genetic concepts and metallotects. Aust. J. Earth Sci. 44, 317–328.

Brown, A.C., 1992. Sediment-hosted stratiform copper deposits. Geosci. Canada, 19.

Cailteux, J., Kampunzu, A., Lerouge, C., Kaputo, A., Milesi, J., 2005. Genesis of sediment-hosted stratiform copper–cobalt deposits, central African Copperbelt. J. Afr. Earth Sci. 42, 134–158.

Cen, B.X., (in Chinese) 1993. The mineralization regularity and exploration model system of Hu-Bi type copper mineral in Zhongtiao Mountains, Shanxi. China University of Geosciences Press, Wuhan, pp. 37–53.

Chi, G., Xue, C., 2011. Abundance of CO_2-rich fluid inclusions in a sedimentary basin-hosted Cu deposit at Jinman, Yunnan, China: implications for mineralization environment and classification of the deposit. Miner. Depos. 46, 365–380.

Chi, G.X., Ni, P., 2007. Equations for calculation of NaCl/(NaCl + $CaCl_2$) ratios and salinities from hydrohalite-melting and ice-melting temperatures in the H_2O–NaCl–$CaCl_2$ system. Acta Petrol. Sin. 23, 33–37.

Compilation Group of the Geology of Copper Deposits of the Zhongtiao Mountains, 1978. Geology of Copper Deposits in the Zhongtiao Mountains. Geological Publishing House, Beijing, pp. 25–86 (in Chinese).

Coplen, T.B., Kendall, C., Hopple, J., 1983. Comparison of stable isotope reference samples. Nature 302, 236–238.

Crerar, D.A., Barnes, H., 1976. Ore solution chemistry: V. Solubilities of chalcopyrite and chalcocite assemblages in hydrothermal solution at 200 °C to 350 °C. Econ. Geol. 71, 772–794.

Du, L.L., Yang, C.H., Guo, J.H., Wang, W., Ren, L.D., Wan, Y.S., Geng, Y.S., 2010. The age of the base of the Paleoproterozoic Hutuo Group in the Wutai Mountains area, North China Craton: SHRIMP zircon U–Pb dating of basaltic andesite. Chinese Sci Bull. 55, 1782–1789.

Du, L.L., Yang, C.H., Wang, W., Ren, L.D., Wan, Y.S., Wu, J.S., Zhao, L., Song, H.X., Geng, Y.S., Hou, K.J., 2012. Paleoproterozoic rifting of the North China Craton: geochemical and zircon Hf isotopic evidence from the 2137 Ma Huangjinshan A-type granite porphyry in the Wutai area. J. Asian Earth Sci. 72, 190–202.

El Desouky, H.A., Muchez, P., Cailteux, J., 2009. Two Cu–Co sulfide phases and contrasting fluid systems in the Katanga Copperbelt, Democratic Republic of Congo. Ore Geol. Rev. 36, 315–332.

El Desouky, H.A., Muchez, P., Boyce, A.J., Schneider, J., Cailteux, J.L., Dewaele, S., von Quadt, A., 2010. Genesis of sediment-hosted stratiform copper–cobalt mineralization at Luiswishi and Kamoto, Katanga Copperbelt (Democratic Republic of Congo). Miner. Depos. 45, 735–763.

Goodfellow, W., Lydon, J., 2007. Sedimentary Exhalative (SEDEX) Deposits. Mineral Deposits of Canada: A Synthesis of Major Deposit Types, District Metallogeny, the Evolution of Geological Provinces, and Exploration Methods: Geological Association of Canada. Mineral Deposits Division, pp. 163–183, Special Publication.

Goldstein, R.H., Reynolds, T.J., 1994. Systematic of fluid inclusions in diagenetic materials. Soc. Sediment. Geol. Short Course 31, 199.

Hitzman, M., Kirkham, R., Broughton, D., Thorson, J., Selley, D., 2005. The sediment-hosted stratiform copper ore system. Econ. Geol. 100th Anniversary, 609–642.

Hitzman, M.W., Selley, D., Bull, S., 2010. Formation of sedimentary rock-hosted stratiform copper deposits through Earth history. Econ. Geol. 105, 627–639.

Holland, H.D., 1972. Granites, solutions, and base metal deposits. Econ. Geol. 67, 281–301.

Holland, H.D., Malinin, S.D., 1979. The solubility and occurrence of non-ore minerals. Geochem. Hydrotherm. Ore Depos. 2, 461–508.

Huang, C.K., Bai, Y., Zhu, Y.S., Wang, H.Z., Shang, X.Z., 2001. Copper Deposit of China. Geological Publishing House, Beijing, pp. 142–152.

Huang, W.P., Sun, F.Y., Zhang, H., Wang, J.L., 2013. Petrology and geochemistry characteristic of Hu-Bi copper deposit in Zhongtiao mountains of Shanxi Province. Glob. Geol. 32, 212–220 (in Chinese with English abstract).

Hu, W.X., Sun, D.Z., 1987. Mineralization and evolution of the early proterozoic copper deposits in the Zhongtiao Mountains. Acta Geol. Sin., 152–165 (in Chinese with English abstract).

Huston, D.L., Pehrsson, S., Eglington, B.M., Zaw, K., 2010. The geology and metallogeny of volcanic-hosted massive sulfide deposits: Variations through Geologic Time and with Tectonic Setting. Econ. Geol. 105 (3), 571–591.

Jiang, Y.H., Niu, H.C., Bao, Z.W., Li, N.B., Shan, Q., Yang, W.B., 2013a. Fluid evolution of the Tongkuangyu porphyry copper deposit in the Zhongtiaoshan region: evidence from fluid inclusions. Ore Geol. Rev. 63, 498–509.

Jiang, Y.H., Luo, Y., Niu, H.C., Guo, S.L., Li, N.B., 2013b. Study on fluid inclusions from the Luojiahe copper deposit in Zhongtiaoshan region. Acta Petrol. Sin. 29 (7), 2583–2592 (in Chinese with English abstract).

Land, L.S., Milliken, K.L., 1981. Feldspar diagenesis in the Frio Formation, Brazoria County, Texas Gulf Coast. Geology 9, 314–318.

Leach, D.L., Bradley, D.C., Huston, D., Pisarevsky, S.A., Taylor, R.D., Gardoll, S.J., 2010. Sediment-hosted lead–zinc deposits in Earth history. Econ. Geol. 105, 593–625.

Lecumberri-Sanchez, P., Steele-MacInnis, M., Bodnar, R.J., 2012. A numerical model to estimate trapping conditions of fluid inclusions that homogenize by halite disappearance. Geochim. Cosmochim. Acta 92, 14–22.

Li, Y., Audétat, A., Lerchbaumer, L., Xiong, X., 2009. Rapid Na, Cu exchange between synthetic fluid inclusions and external aqueous solutions: evidence from LA–ICP-MS analysis. Geofluids 9, 321–329.

Liu, C.H., Zhao, G.C., Sun, M., Zhang, J., Yin, C., 2012. U–Pb geochronology and Hf isotope geochemistry of detrital zircons from the Zhongtiao Complex: constraints on the tectonic evolution of the Trans-North China Orogen. Precambrian Res. 222–223, 159–172.

Lowenstern, J.B., 2001. Carbon dioxide in magmas and implications for hydrothermal systems. Miner. Depos. 36, 490–502.

Melezhik, V.A., Fallick, A.E., Medvedev, P.V., Makarikhin, V.V., 1999. Extreme 13Ccarb enrichment in ca. 2.0 Ga magnesite–stromatolite–dolomite–red beds' association in a global context: a case for the world-wide signal enhanced by a local environment. Earth-Sci. Rev. 48, 71–120.

Moore, J., 2010. Comparative study of the Onganja copper mine, Namibia: a link between Neoproterozoic mesothermal Cu (–Au) mineralization in Namibia and Zambia. South Afr. J. Geol. 113, 445–460.

Oakes, C.S., Bodnar, R.J., Simonson, J.M., 1990. The system NaCl–$CaCl_2$–H_2O: I. The ice liquidus at 1 atm total pressure. Geochim. Cosmochim. Acta 54, 603–610.

Oliver, N.H., Rawling, T.J., Cartwright, I., Pearson, P.J., 1994. High-temperature fluid-rock interaction and scapolitization in an extension-related hydrothermal system, Mary Kathleen, Australia. J. Petrol. 35, 1455–1491.

O'Neil, J.R., Clayton, R.N., Mayeda, T.K., 1969. Oxygen isotope fractionation in divalent metal carbonates. J. Chem. Phys. 51, 5547.

Pang, X.J., (Master thesis) 2010. Study on the Enrichment Regularities and the Ore Genetic Rules of Nanhegou and Laobaotan Copper Deposits in Zhongtiao Mountains, Shanxi Province. JiLin University, pp. 67–91 (in Chinese with English abstract).

Pirajno, F., 2009. Hydrothermal Processes and Mineral Systems. Springer.

Pollard, P.J., 2001. Sodic (–calcic) alteration in Fe-oxide–Cu–Au districts: an origin via unmixing of magmatic H_2O–CO_2–NaCl ± $CaCl_2$–KCl fluids. Mineral. Depos. 36, 93–100.

Robb, L., 2009. Introduction to Ore-forming Processes. Wiley.com.

Roedder, E., 1971. Fluid inclusion studies on the porphyry-type ore deposits at Bingham, Utah, Butte, Montana, and Climax, Colorado. Econ. Geol. 66, 98–118.

Roedder, E., 1984. Fluid inclusions. Rev. Mineral. 12, 646.

Rose, A., 1976. The effect of cuprous chloride complexes in the origin of red-bed copper and related deposits. Econ. Geol. 71, 1036–1048.

Selley, D., Broughton, D., Scott, R., Hitzman, M., Bull, S., Large, R., McGoldrick, P., Croaker, M., Pollington, N., 2005. A New Look at the Geology of the Zambian Copperbelt.

Seo, J.H., Heinrich, C.A., 2013. Selective copper diffusion into quartz-hosted vapor inclusions: evidence from other host minerals, driving forces, and consequences for Cu–Au ore formation. Geochim. Cosmochim. Acta 113, 60–69.

Singer, D.A., 1995. World class base and precious metal deposits; a quantitative analysis. Econ. Geol. 90, 88–104.

Sun, D.Z., Hu, W.X., 1993. Precambrian Geochronology, Chronotectonic Framework and Model of Chronocrustal Structure of the Zhongtiao Mountains, 1st ed. Geological publishing house, Beijing, pp. 1–102 (in Chinese).

Sun, H.T., Ge, C.H., 1990. Hydrothermal Exhalative Copper Deposits in Zhongtiaoshan District, Shanxi Province, 1st ed. Beijing Science and Technology Press, Beijing, pp. 101-106 (in Chinese with English abstract).

Sun, J.Y., Ji, S.K., Zhen, Y.Q., 1995. The Copper Deposits in the Zhongtiao Rift, 1st ed. Geological publishing house, Beijing, pp. 84–140 (in Chinese).

Tian, W., Liu, S.W., Zhang, H.F., 2006. Paleoproterozoic potassic granitoids in the sushui complex from the Zhongtiao Mountains, Northern China: geochronology, geochemistry and petrogenesis. Acta Geol. Sin.-Engl. Ed. 80, 875–885.

Ulrich, T., Heinrich, C.A., 2001. Geology and alteration geochemistry of the porphyry Cu–Au deposit at Bajo de la Alumbrera Argentina. Econ. Geol. 96, 1719–1742.

Wan, Y., Xie, S., Yang, C., Kröner, A., Ma, M., Dong, C., Du, L, Xie, H., Liu, D., 2014. Early Neoarchean (~2.7 Ga) tectono-thermal events in the North China Craton: a synthesis. Precambrian Res. 247, 45–63.

Wei, D.Y., Xing, S.C., Liang, X., 1984. The implications of the Hu-Bi type copper deposits in the Zhongtiaoshan region. Acta Hebei Geol. Coll. 25, 30–41 (in Chinese).

Xu, Q.L., (Master thesis) 2010. Study on the Geological Characteristics and Ore Genesis of Tongkuangyu Copper Deposit in the Zhongtiaoshan Mountains, Shanxi Province. Jilin University, pp. 59–71 (in Chinese with English abstract).

Zajacz, Z., Seo, J.H., Candela, P.A., Piccoli, P.M., Tossell, J.A., 2011. The solubility of copper in high-temperature magmatic vapors: a quest for the significance of various chloride and sulfide complexes. Geochim. Cosmochim. Acta 75, 2811–2827.

Zhai, M.G., Santosh, M., 2011. The early Precambrian odyssey of the North China Craton: a synoptic overview. Gondwana Res. 20, 6–25.

Zhai, M.G., Li, T.S., Peng, P., Hu, B., Liu, F., Zhang, Y., 2010. Precambrian Key Tectonic Events and Evolution of the North China Craton, vol. 338. Geological Society, London, pp. 235–262, Special Publications.

Zhai, M.G., Santosh, M., 2013. Metallogeny of the North China Craton: link with secular changes in the evolving Earth. Gondwana Res. 24, 275–297.

Zhang, H., (PhD thesis) 2012. Metallogenesis of Paleoproterozoic Copper Deposits in the Northern Zhongtiaoshan Mountains, Shanxi Province. JiLin University, pp. 119–123 (in Chinese with English abstract).

Zhao, B., Wang, D.H., Hou, K.J., Liu, R.L., 2012a. Isochronology study on Sushui Complex in Zhongtiao Mountains and its geological significance. J. Earth Sci. Environ. 34, 1–8 (in Chinese with English abstract).

Zhao, G., Wilde, S.A., Cawood, P.A., Sun, M., 2001. Archean blocks and their boundaries in the North China Craton: lithological, geochemical, structural and P–T path constraints and tectonic evolution. Precambrian Res. 107, 45–73.

Zhao, X.-F., Zhou, M.-F., Hitzman, M.W., Li, J.-W., Bennett, M., Meighan, C., Anderson, E., 2012b. Late Paleoproterozoic to early Mesoproterozoic Tangdan sedimentary rock-hosted strata-bound copper deposit, Yunnan Province, Southwest China. Econ. Geol. 107, 357–375.

Zhen, Y.Q., Du, J.S., Liu, L.L., Wang, Y.H., 1995. Physicochemical condition of mineralizing fluids in copper ore deposit, the Zhongtiaoshan rift zone. J. Guilin Inst. Technol. 15, 113–123 (in Chinese with English abstract).

Zhen, Y.Q., 1997. On the ages of copper mineralizations in the Zhongtiao rift zone. J. GuiLin Inst. Technol. 17, 307–315 (in Chinese with English abstract).

Zheng, Y.F., 1990. Carbon–oxygen isotopic covariation in hydrothermal calcite during degassing of CO_2. Miner. Depos. 25, 246–250.

Zheng, Y.F., Chen, J.F., 2000. Stable Isotope Geochemistry, 1st ed. Science Press, Beijing, pp. 291–296.

Zhu, X., Zhai, M., Chen, F., Lyu, B., Wang, W., Peng, P., Hu, B., 2013. ~2.7-Ga crustal growth in the North China Craton: evidence from zircon U–Pb ages and Hf isotopes of the sushui complex in the Zhongtiao Terrane. J. Geol. 121, 239–254.